Impact of Relay Placement in Three-Hop Buffer-Aided FSO Systems: An Approximate Performance Analysis Approach

Mirna El-Rajab and Chadi Abou-Rjeily

Abstract

In this paper, we consider the problem of three-hop Free Space Optical (FSO) communications in the context of decode-and-forward (DF) buffer-aided (BA) relaying where the two relays are equipped with buffers of finite size. We adopt a Markov chain analysis for evaluating the outage probability (OP) and average packet delay (APD) of the considered serial relaying system that operates naturally in the full-duplex (FD) mode. Given the large number of states involved in the analysis and the large number of associated transitions resulting from the FD operation, we establish an approximate performance analysis approach following from the intractability of an exact analysis. The suggested framework improves over the existing asymptotic studies and provides closed-form approximate OP and APD expressions that are extremely close to the exact expressions in the average-to-high signal-to-noise ratio (SNR) range. Simulations over gamma-gamma atmospheric turbulence channels highlight on the accuracy of the adopted approximate approach irrespective of the underlying network setup. This accuracy is particularly appealing for predicting the APD performance since the gap between the exact APD and the existing asymptotic APD bounds can be huge for FSO networks with comparable hop distances.

Index Terms

Free-Space Optics, FSO, multi-hop, serial relaying, performance analysis, outage probability, queuing delay, Markov chain.

I. Introduction

In order to meet the ever-increasing demand for communication speed and reliability, cooperation, which is a human-like behavior, has been adopted in communication systems mainly through

The authors are with the Department of Electrical and Computer Engineering of the Lebanese American University (LAU), Byblos, Lebanon. (e-mails: mirna.elrajab@lau.edu and chadi.abourjeily@lau.edu.lb).

Cooperative Relaying (CR). This technique allows a source to communicate with its respective destination through relays. In this way, diversity can be increased as more paths become available for signal propagation and path-loss can be decreased as the transmitting nodes become closer to the receiving nodes [1].

Traditional Radio Frequency (RF) backhauling techniques (i.e. microwave links) no longer meet the growing demand of higher data rates due to their expensive deployment costs and small bandwidths following from the scarcity of the RF spectrum. Thus, Free Space Optical (FSO) communications emerged as a promising solution to the “last mile” problem due to its high data rate capacity and wide-bandwidth [2], [3]. The FSO technology has been recently investigated for a wide variety of applications ranging from fronthauling/backhauling to disaster recovery [3]. However, FSO communications require a line-of-sight (LOS) path and, thus, are highly affected by the weather where certain atmospheric conditions, as rain and fog, attenuate the signal. Accordingly, the overall system performance is deteriorated in terms of outage probability (OP), error probability and ergodic capacity [2], [4]. In order to compensate for the unpredictability of the FSO links, hybrid FSO/RF solutions were investigated where a backup RF link is deployed in parallel with the FSO link [2]. This solution stemmed from the fact that the FSO links’ deficiencies are triggered by phenomena different from that of the RF links. As such, when the FSO link is in outage, the RF link will be activated and therefore the system will take advantage of the high data rates provided by the FSO links, in addition to the RF link’s reliability [2]. The deployment of relays has also served as a mean to mitigate the atmospheric limiting effects by enhancing the diversity orders and communication ranges of FSO communication systems [5], [6].

For RF communications, the deployed relays could operate either in the half-duplex (HD) mode or the full-duplex (FD) mode. Unlike HD relaying, FD relays can transmit and receive concurrently in the same time slot thus enhancing the spectral efficiency at the expense of increased levels of self-loop-interference [1], [7]. On the other hand, FSO relays operate naturally in the FD mode where the optical beam falling on the relay’s photo-detector does not interfere with the beam transmitted from the relay’s laser following from the high directivity of the LOS FSO links [6]. In this case, signal detection and signal transmission are handled by different optical components and, hence, the relay can receive and transmit at the same time. The literature on FD FSO relaying is extensive especially in the context of buffer-free (DF) relaying [8]–[12]. For BF relaying, the decode-and-forward (DF) relay decodes and retransmits the received information packets without possessing any buffering capabilities at the physical layer.

While conventional BF relaying constitutes the most widely researched cooperation model, recent studies shed light on the benefits that can be reaped from equipping the relays with buffers whether in the context of RF communications [13]–[17] or FSO communications [18], [19]. In the framework of buffer-aided (BA) relaying, it has been proven in the aforementioned references that employing buffers enhances both the throughput and diversity at the expense of increased average packet delays (APD). In BA systems, the information packets are stored until the channel conditions become more favorable thus reducing the OP. Comparing the employment of buffers with time diversity methods established on packet interleaving and network coding, it can be observed that BA relaying does not lead to data-rate loss nor complex dual encoding/decoding at the expense of a trivial cost increase required to integrate buffers at the relays [20]. The RF max-max scheme was proposed in [13] in order to improve the performance of the max-min protocol where the same relay is picked for both reception and transmission. In comparison, the RF max-max strategy refers to a two-slot protocol where the relay with the best S-R link is chosen for reception in the first time slot and that with the best R-D link is chosen for transmission in the subsequent time slot. This will reduce the OP as the presence of buffers will guarantee that different relays can be selected for reception and transmission. Aiming to leverage the fixed two-slot allocation, the RF max-link scheme allows the communication to take place along the strongest link selected among all the available S-R and R-D links and thus doubling the diversity gain as compared to both max-min and max-max schemes [14]. The problem of packet delay was investigated in [15] where a scheme has been proposed aiming to lower the APD by assigning a higher priority to R-D links as compared to the S-R links and thus emptying the buffers at a faster pace. Further improvements on the max-link scheme were introduced in [16] and this latter scheme was extended to the setup of amplify-and-forward (AF) relaying in [17].

In the context of DF FSO cooperative communications, BA parallel relaying and BA serial relaying were investigated in [20] and [21], respectively. In [20], several relaying protocols were studied and compared for FSO networks with an arbitrary number of relays, each equipped with a buffer of finite size. Similarly, in [21], a DF multi-hop BA FSO communication system with finite-size buffers was investigated in terms of the OP and APD performance. Among the different relaying techniques, serial relaying (or multi-hop communication) has drawn a lot of attention especially for extending the coverage FSO networks in the scenarios where the S-D distance is extremely long. Compared to conventional single-hop communications, the multi-hop setup provides a number of benefits such as enhanced energy-efficiency, prolonged coverage, better link performance, improved throughput, simplicity and prominent flexibility of network planning [21]. While BF-AF-FSO serial relaying and BF-DF-FSO serial relaying were studied in [22], [23] and [24], [25], respectively, this relaying scheme has been extended to the scenario of BA-DF-FSO communications in [21] as previously delineated.

For BA-DF-FSO systems with two or more relays, the OP and APD were derived using an asymptotic approach that holds for large values of the signal-to-noise ratio (SNR) as exact solutions were out of reach [21]. This is due to the large number of states in the Markov chain and the several possible transitions stemming from the full-duplexity of the system. Moreover, the asymptotic OP and APD expressions derived in [21] are limited to the scenario where the constituent hop distances are remarkably different. The aim of this work is to leverage the solution obtained in [21] and reach an approximate solution that holds for a wider range of SNRs for a three-hop system while relaxing all constraints on the network setup. The proposed approximate performance analysis framework revolves around the identification of a closed set comprising 12 states out of the $(L+1)^2$ states for buffers of size L where, at steady-state, the Markov chain is within this set with a probability approaching 1. This closed-set is further divided into 3 quasi-closed subsets (comprising 4 states each) where we derive the approximate steady state transitions between the different subsets and between the states of the same subset. The selection of the closed set and its subsequent partitioning into 3 subsets will vary depending on which hop of the three hops is the bottleneck link. The proposed calculation methodology significantly simplifies the theoretical analysis resulting in closed-form approximate OP and APD expressions that accurately predict the performance of three-hop BA networks over a wide range of SNR values.

The remainder of this paper is structured as follows. First, the system model and other preliminaries adopted for this study are given in Section II. In Section III, we derive the APD and OP expressions using an approximate approach for three different cases arising from the relays' placement. Subsequently, simulation results are provided in Section IV with the aim of comparing the approximate results and exact results. Finally, conclusions are provided in Section V.

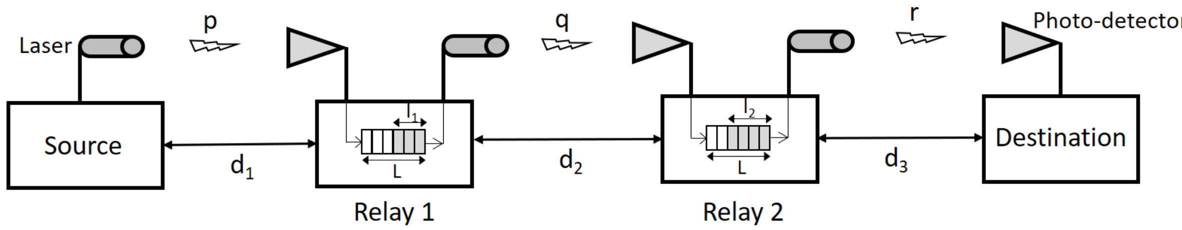

Fig. 1. Three-hop buffer-aided FSO system.

II. System Model and Preliminaries

A. Basic Parameters

We consider a 3-hop FSO communication system with intensity-modulation and direct-detection (IM/DD) corrupted by additive white Gaussian noise (AWGN). The source (S) communicates with the destination (D) through 2 decode-and-forward (DF) relays placed in series denoted by R_1 and R_2, respectively. Each relay is equipped with a buffer (data queue) of size L. We assume that there is no direct link available between S and D. Thus, for a packet to be communicated successfully, it should traverse all three indirect hops S-R$_1$, R$_1$-R$_2$ and R$_2$-D of lengths d_1, d_2 and d_3, respectively. The system model is depicted in Fig. 1.

We assume that the FSO channels are affected by gamma-gamma turbulence-induced scintillation along with pointing errors. The outage probabilities along the S-R$_1$, R$_1$-R$_2$ and R$_2$-D links are given by [21], [26]:

$$p = \frac{\xi_1^2}{\Gamma(\alpha_1)\Gamma(\beta_1)} G_{2,4}^{3,1}\left[\frac{\alpha_1\beta_1}{G_1 P_M/3}\middle|\begin{matrix} 1, \xi_1^2+1 \\ \xi_1^2, \alpha_1, \beta_1, 0\end{matrix}\right] \tag{1}$$

$$q = \frac{\xi_2^2}{\Gamma(\alpha_2)\Gamma(\beta_2)} G_{2,4}^{3,1}\left[\frac{\alpha_2\beta_2}{G_2 P_M/3}\middle|\begin{matrix} 1, \xi_2^2+1 \\ \xi_2^2, \alpha_2, \beta_2, 0\end{matrix}\right] \tag{2}$$

$$r = \frac{\xi_3^2}{\Gamma(\alpha_3)\Gamma(\beta_3)} G_{2,4}^{3,1}\left[\frac{\alpha_3\beta_3}{G_3 P_M/3}\middle|\begin{matrix} 1, \xi_3^2+1 \\ \xi_3^2, \alpha_3, \beta_3, 0\end{matrix}\right], \tag{3}$$

where $\Gamma(\cdot)$ designates the Gamma function and $G_{p,q}^{m,n}[\cdot]$ is the Meijer G-function. Moreover, $(\alpha_1, \beta_1) \triangleq (\alpha(d_1), \beta(d_1))$, $(\alpha_2, \beta_2) \triangleq (\alpha(d_2), \beta(d_2))$
and $(\alpha_3, \beta_3) \triangleq (\alpha(d_3), \beta(d_3))$ refer to the parameters of the gamma-gamma distribution associated

with the three hops S-R$_1$, R$_1$-R$_2$ and R$_2$-D, respectively. These parameters can be determined from:

$$\alpha(d) = \left[\exp\left(0.49\sigma_R^2(d)/(1+1.11\sigma_R^{12/5}(d))^{7/6}\right)-1\right]^{-1} \tag{4}$$

$$\beta(d) = \left[\exp\left(0.51\sigma_R^2(d)/(1+0.69\sigma_R^{12/5}(d))^{5/6}\right)-1\right]^{-1}, \tag{5}$$

where the Rytov variance is $\sigma_R^2(d) = 1.23C_n^2 k^{7/6} d^{11/6}$ with C_n^2 and k symbolizing the refractive index structure parameter and wave number, respectively.

In (1)-(3), P_M indicates the optical power margin with respect to the detection signal-to-noise ratio (SNR) threshold. In other words, the actual SNR is equal to P_M multiplied by the detection SNR threshold. As such, $P_M \geq 1$ (or, in decibels, $P_M \geq 0$ dB) so that the actual SNR exceeds the threshold SNR in order to ensure that the information message is decoded with an arbitrarily small probability of error. For example, in Section IV, we consider the values of P_M ranging from 0 dB to 30 dB. In (1)-(3), P_M is divided by the number of hops (that is equal to three). This follows from evenly splitting the power among the constituent hops ensuring the same transmission power as in non-cooperative point-to-point communications.

In (1)-(3), the parameter ξ_n (for $n = 1, 2, 3$) is associated with pointing errors and can be computed from $\xi_n = \omega_{z_{eq},n}/2\sigma_{s,n}$ where $\sigma_{s,n}$ stands for the pointing error displacement standard deviation at the receiver of the n-th hop and:

$$\omega_{z_{eq},n}^2 = \omega_{z,n}^2 \sqrt{\pi} \mathrm{erf}(v_n) / \left[2v_n e^{-v_n^2}\right]. \tag{6}$$

In (6), $\omega_{z,n}$ represents the beam waist along the n-th hop and $v_n = \sqrt{\pi/2}(a_n/\omega_{z,n})$ where erf$\,(\cdot)$ indicates the error function and a_n refers to the receiver's radius at the traversed hop. Finally, G_1, G_2 and G_3 designate the gains resulting from the possibility of having the corresponding indirect links shorter than the direct link of distance d_{SD}:

$$G_n = \left(\frac{A_n}{A_{\mathrm{SD}}}\right)\left(\frac{\xi_{\mathrm{SD}}^2+1}{\xi_{\mathrm{SD}}^2}\right) e^{-\sigma(d_n - d_{\mathrm{SD}})} \quad ; \quad n = 1, 2, 3, \tag{7}$$

where σ is the attenuation coefficient, $A_n = \mathrm{erf}^2(v_n)$ while A_{SD} and ξ_{SD} are the pointing error parameters associated with the direct link S-D.

In order to highlight on the performance gains that can be reaped from multi-hop relaying systems, these systems are customarily matched against the benchmark non-cooperative communications where S and D communicate directly with no relays placed in between. As such, even though a direct link is not assumed between S and D in the adopted system model, yet the parameters $\xi_{\rm SD}$, $A_{\rm SD}$ and $d_{\rm SD}$ appear in the formulation provided in (7). In fact, the parameter P_M is formally defined as the power margin (above the detection threshold) measured at D corresponding to a signal transmitted from S. In other words, P_M is considered for a reference distance $d_{\rm SD}$ (with pointing error parameters $\xi_{\rm SD}$ and $A_{\rm SD}$) implying that the effective power margin for the n-th hop of distance d_n (with pointing error parameters ξ_n and A_n) is $\frac{G_n P_M}{N}$ where G_n is given in (7) while N is the number of hops. This relation highlights the fact that, with respect to non-cooperative communications, the power margin is enhanced by a factor G_n and reduced by a factor N. As such, placing more relays between S and D will result in shorter hops (G_n increases contributing positively to the SNR) with a smaller fraction of the total power allocated to each hop (N increases contributing negatively to the SNR). This normalisation is essential for comparing systems with different numbers of hops (or relays) as is carried out in Section IV where we compare 1-hop, 2-hop and 3-hop systems. Finally, from Fig. 1, it can be observed that a direct link between S and D might not be available even if $d_{\rm SD}$ is relatively small since establishing this link necessitates placing an additional laser at S and an additional photo-detector at D. Therefore, the implementation of the proposed solution necessitates 3 lasers and 3 photo-detectors while an alternative system model with a direct link necessitates 4 lasers and 4 photo-detectors.

Various statistical models have been proposed over the years for modeling atmospheric turbulence. For the weak and strong turbulence conditions, the lognormal and negative exponential distributions are often considered, respectively [27]. Recently, the gamma-gamma distribution has received considerable attention because of its excellent fit with measurement data for a wide range of turbulence conditions (ranging from weak to strong turbulence). For this reason, the gamma-gamma scintillation model is adopted in this paper.

It is worth highlighting that the underlying distribution will only affect the specific values of the outage probabilities in (1)-(3) without altering the subsequent calculation methodology for deriving the performance metrics of the 3-hop BA system. More specifically, the derived OP and APD approximate closed-form expressions reported in Section III will hold for all values of the hops' outage probabilities p, q and r regardless of how these probabilities are related to the adopted scintillation model. Consequently, the analysis presented in this paper can be applied with all scintillation distributions and, in particular, with the Malaga distribution that was recently proposed as a unifying distribution for modeling atmospheric turbulence [27]. In this case, the single-term outage probabilities in (1)-(3) will be simply replaced by a weighted sum of multiple terms that have the same form (refer to eq. (11) in [28]). It is worth noting that the performance analysis with the Malaga distribution often assumes that the channel parameter β in (5) is a natural number since, otherwise, the density function will involve an infinite summation thus incurring a high degree of freedom on the distribution [27], [28]. Therefore, the adopted gamma-gamma model is better adapted for capturing the dependence of the performance metrics on the placement of the relays that constitutes a central parameter that characterizes relaying networks. In fact, in this work, no assumptions are made on the value of β that can be directly related to the underlying link distance according to (5).

B. FD Relaying Strategy

The FSO relays operate naturally in the full-duplex (FD) mode where the optical signals received at the photo-detector and transmitted from the laser do not interfere with each other. Consequently, all nodes in the network can simultaneously transmit and receive where the dedicated and highly-directive LOS FSO links do not interfere with each other. In other words, any relay with a non-full buffer can receive while any relay with a non-empty buffer can transmit where concurrent transmissions can take place from R_1 and R_2 (as well as S). In what follows, the numbers of packets present in the buffers of R_1 and R_2 will be denoted by l_1 and l_2, respectively, where $0 \leq l_1 \leq L$ and $0 \leq l_2 \leq L$.

C. Transition Probabilities

A Markov chain (MC) approach will be utilized to examine the considered FSO BA system where a state of the MC depicts the numbers of packets in the buffers of the relays and is designated by $\mathbf{l} \triangleq (l_1, l_2)$. Denote by $\mathbf{A}$ the state transition matrix defined as the $(L+1)^2 \times (L+1)^2$ matrix where the $((L+1)l_1' + l_2' + 1, (L+1)l_1 + l_2 + 1)$-th element of $\mathbf{A}$ is expressed as $t_{\mathbf{l},\mathbf{l}'}$ which refers to the probability of moving from state $\mathbf{l}$ to state $\mathbf{l}'$.

The transition probabilities corresponding to the three-hop FD scheme were derived in [21] in seven different cases depending on the values of l_1 and l_2. For the sake of completeness, these probabilities are reported in Table I. It is worth highlighting that deriving the transition probabilities does not constitute a contribution of this paper that focuses on using these probabilities to derive more accurate OP and APD performance metrics.

TABLE I

THE TRANSITION PROBABILITIES OF THE THREE-HOP FD SYSTEM (DIVIDED INTO EIGHT CASES). IN THIS TABLE, $\bar{p} = 1 - p$, $\bar{q} = 1 - q$ AND $\bar{r} = 1 - r$.

Cases	$\mathbf{l} = (0,0)$	$\mathbf{l} = (L,0)$	$\mathbf{l} = (L,L)$	$\mathbf{l} = (l_1,0)$ $l_1 = 1, ..., L-1$
$t_{\mathbf{l},\mathbf{l}'}$	$t_{(0,0),(0,0)} = p$ $t_{(0,0),(1,0)} = \bar{p}$	$t_{(L,0),(L,0)} = q$ $t_{(L,0),(L-1,1)} = \bar{q}$	$t_{(L,L),(L,L)} = r$ $t_{(L,L),(L,L-1)} = \bar{r}$	$t_{(l_1,0),(l_1,0)} = pq$ $t_{(l_1,0),(l_1,1)} = \bar{p}\bar{q}$ $t_{(l_1,0),(l_1+1,0)} = \bar{p}q$ $t_{(l_1,0),(l_1-1,1)} = p\bar{q}$
Cases	$\mathbf{l} = (L,l_2)$ $l_2 = 1, ..., L-1$	$\mathbf{l} = (0,l_2)$ $l_2 = 1, ..., L$	$\mathbf{l} = (l_1,L)$ $l_1 = 1, ..., L-1$	$\mathbf{l} = (l_1,l_2)$ $l_1, l_2 = 1, ..., L-1$
$t_{\mathbf{l},\mathbf{l}'}$	$t_{(L,l_2),(L,l_2)} = qr$ $t_{(L,l_2),(L-1,l_2)} = \bar{q}\bar{r}$ $t_{(L,l_2),(L,l_2-1)} = q\bar{r}$ $t_{(L,l_2),(L-1,l_2+1)} = \bar{q}r$	$t_{\mathbf{l},\mathbf{l}} = pr$ $t_{\mathbf{l},\mathbf{l}+(1,0)} = \bar{p}r$ $t_{\mathbf{l},\mathbf{l}+(0,-1)} = p\bar{r}$ $t_{\mathbf{l},\mathbf{l}+(1,-1)} = \bar{p}\bar{r}$	$t_{\mathbf{l},\mathbf{l}} = pr$ $t_{\mathbf{l},\mathbf{l}+(1,0)} = \bar{p}r$ $t_{\mathbf{l},\mathbf{l}+(0,-1)} = p\bar{r}$ $t_{\mathbf{l},\mathbf{l}+(1,-1)} = \bar{p}\bar{r}$	$t_{\mathbf{l},\mathbf{l}} = prq + \bar{p}\bar{q}\bar{r}$ $t_{\mathbf{l},\mathbf{l}+(-1,0)} = p\bar{q}\bar{r}$ $t_{\mathbf{l},\mathbf{l}+(1,-1)} = \bar{p}q\bar{r}$ $t_{\mathbf{l},\mathbf{l}+(0,1)} = \bar{p}\bar{q}r$ $t_{\mathbf{l},\mathbf{l}+(1,0)} = \bar{p}qr$ $t_{\mathbf{l},\mathbf{l}+(-1,1)} = p\bar{q}r$ $t_{\mathbf{l},\mathbf{l}+(0,-1)} = pq\bar{r}$

D. Motivation and Contribution

Following from the large number of states in the Markov chain (that is equal to $(L+1)^2$) and from the numerous possible transitions (arising from the full-duplexity of the system), an exact solution to the considered problem seems to be out of reach. Consequently, [21] resorted to an asymptotic analysis that holds for large values of P_M. The aim of this work is to leverage the solution obtained in [21] and to reach an approximate solution that holds for a wider range of values of P_M. In particular, results show that the adopted methodology yields accurate closed-form OP and APD expressions for average-to-high values of P_M.

III. APPROXIMATE PERFORMANCE ANALYSIS

A. Calculation Methodology

The approximate analysis presented in this paper revolves around the identification of a closed-set S where a set S is said to be closed if it satisfies the following condition [21]:

$$t_{\mathbf{l},\mathbf{l}'} = 0 \;\; \forall \;\; \mathbf{l} \in S \;, \; \mathbf{l}' \notin S, \tag{8}$$

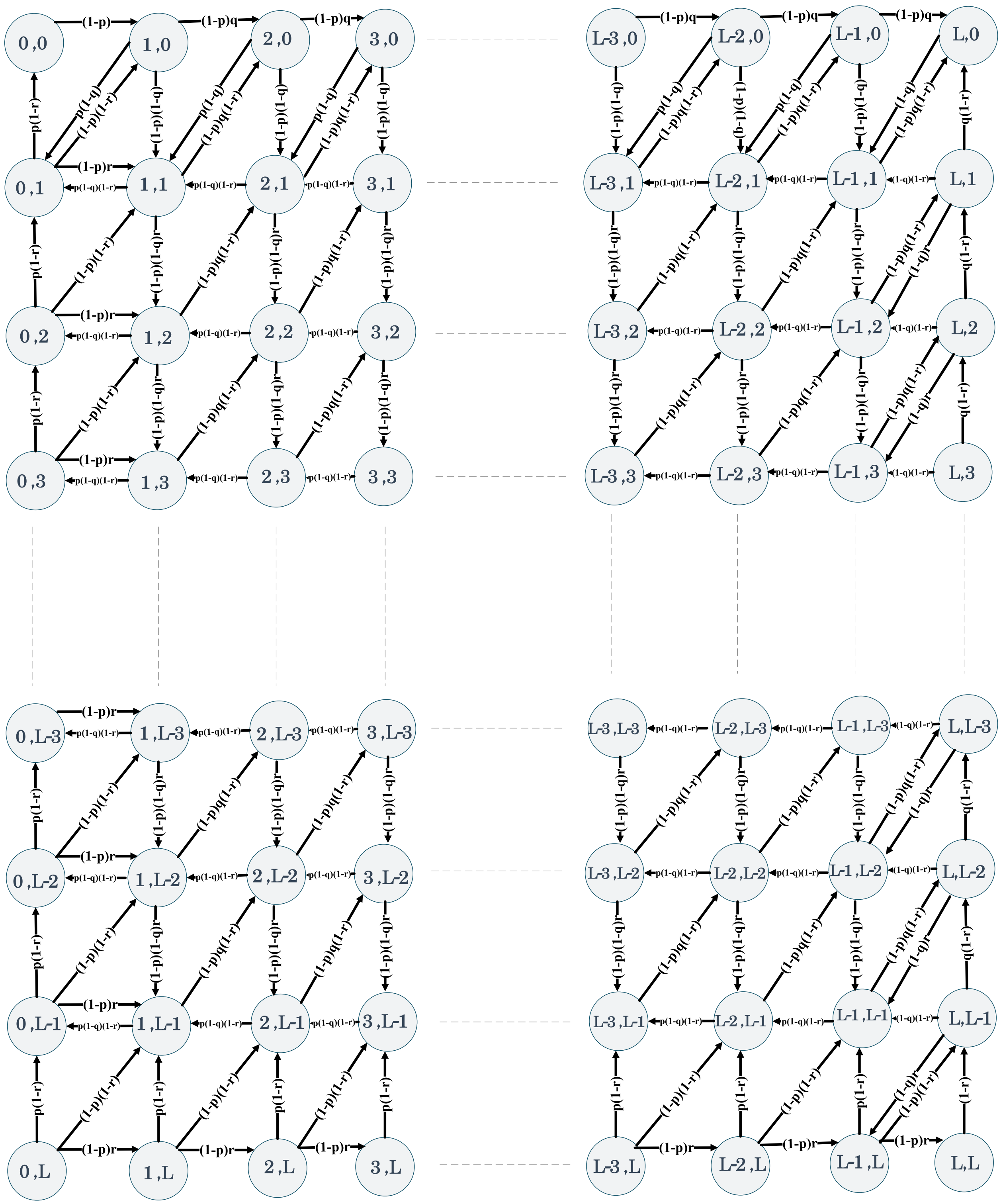

Fig. 2. Approximate Markov Chain State Diagram.

highlighting that no state in S leads to a state outside of S.

Unlike the asymptotic analysis in [21] that identifies a closed-set of 4 states, the approximate analysis in this paper identifies a closed-set of 12 states. This closed-set will be further partitioned into 3 subsets comprising 4 states each: $S = S_1 \cup S_2 \cup S_3$. This partitioning constitutes a key tool for deriving the subsequent closed-form expressions for the steady-state probability distribution.

The probabilities of being in subsets S_1, S_2 and S_3, at steady-state, will be denoted by x, y and z, respectively:

$$\sum_{\mathbf{l} \in S_1} \pi_{\mathbf{l}} = x \quad ; \quad \sum_{\mathbf{l} \in S_2} \pi_{\mathbf{l}} = y \quad ; \quad \sum_{\mathbf{l} \in S_3} \pi_{\mathbf{l}} = z, \tag{9}$$

with $x + y + z = 1$ thus resulting in $\sum_{\mathbf{l} \in S} \pi_{\mathbf{l}} = 1$ where $\pi_{\mathbf{l}}$ stands for the probability of being in state $\mathbf{l}$ at equilibrium.

The first step in the analytical framework consists of evaluating the probabilities x, y and z by considering the transitions between subsets S_1, S_2 and S_3 taken, each, as lumped groups of states. At a second time, the steady-state probability distribution of elements of $S = S_1 \cup S_2 \cup S_3$ can be approximated as follows:

$$\pi_{\mathbf{l}} \approx \begin{cases} \pi_{\mathbf{l}}^{(1)} x, & \mathbf{l} \in S_1; \\ \pi_{\mathbf{l}}^{(2)} y, & \mathbf{l} \in S_2; \\ \pi_{\mathbf{l}}^{(3)} z, & \mathbf{l} \in S_3. \end{cases}, \tag{10}$$

where $\pi_{\mathbf{l}}^{(i)}$ stands for the conditional steady-state probability of being in state $\mathbf{l}$ given that the MC is in subset S_i for $i = 1, 2, 3$. These conditional probabilities satisfy $\sum_{\mathbf{l} \in S_i} \pi_{\mathbf{l}}^{(i)} = 1$ for $i = 1, 2, 3$ and they will be calculated by assuming that the three subsets S_1, S_2 and S_3 are quasi-closed (i.e. the probability of leaving any of these subsets will be neglected when solving for (i): the four probabilities $\{\pi_{\mathbf{l}}^{(1)}, \mathbf{l} \in S_1\}$, (ii): the four probabilities $\{\pi_{\mathbf{l}}^{(2)}, \mathbf{l} \in S_2\}$ and (iii): the four probabilities $\{\pi_{\mathbf{l}}^{(3)}, \mathbf{l} \in S_3\}$).

Finally, for the proposed analytical framework that targets average-to-large values of P_M, the transition probabilities $t_{\mathbf{l},\mathbf{l}'}$ comprising the product of two or more terms of $\{p, q, r\}$ will be neglected. Following from Table I, the simplified MC state diagram is shown in Fig.2.

B. *Steady-State Probabilities*

The closed-set S depends on which hop (among the three hops) constitutes the bottleneck hop. This hop possesses the highest outage probability and corresponds to the link of longest distance under identical scintillation and pointing-error conditions.

1) Bottleneck Link: Hop 1:

Proposition *1:* If the bottleneck link is hop 1 (i.e. $\max\{p,q,r\}=p$), the steady-state probabilities are given by:

$$\begin{cases} \pi_{0,0} &= \frac{p^3(1-q)(1-r)^2}{(p+q+r)c}; \\ \pi_{0,1} &= \frac{p^2(1-p)(1-q)(1-r)}{(p+q+r)c}; \\ \pi_{1,0} &= \frac{p^2(1-p)(1-r)^2}{(p+q+r)c}; \\ \pi_{1,1} &= \frac{p(1-p)^2}{(p+q+r)c}; \\ \pi_{2,0} &= 0; \\ \pi_{2,1} &= \frac{pq(1-q)}{(p+q(1-q)+r)(p-pqr+p^2qr+q-2pq)}; \\ \pi_{3,0} &= \frac{pq^2(1-p)(1-r)}{(p+q(1-q)+r)(p-pqr+p^2qr+q-2pq)}; \\ \pi_{3,1} &= \frac{q^2(1-p)^2}{(p+q(1-q)+r)(p-pqr+p^2qr+q-2pq)}; \\ \pi_{2,2} &= \frac{p^2q(1-q)(1-r)^2}{(p+q+r(1-r))c_1}; \\ \pi_{2,3} &= \frac{pr(1-q)^2(p+r-2pr)}{(p+q+r(1-r))c_1}; \\ \pi_{3,2} &= \frac{pqr(1-p)(1-q)(1-r)}{(p+q+r(1-r))c_1}; \\ \pi_{3,3} &= \frac{qr^2(1-p)^2(1-q)}{(p+q+r(1-r))c_1}, \end{cases} , \tag{11}$$

while all other probabilities $\pi_{l,l'}$ are equal to zero. In (11), $c=p^2r-p^2r^2q+p^2rq-3pr-pq+pqr+pr^2+1$ and $c_1=pqr-pq^2r+4p^2q^2r-5p^2qr-5pqr^2+4pq^2r^2+7p^2qr^2-5p^2q^2r^2+p^2q-p^2q^2+p^2r-2p^2r^2+pr^2+qr^2-q^2r^2$.

Proof: The proof is provided in Appendix A. This proof is based on the partitioning of the identified closed-set S as $S=S_1\cup S_2\cup S_3$ with:

$$S_i=\begin{cases} \{(0,0),(0,1),(1,0),(1,1)\}, & i=1; \\ \{(2,0),(2,1),(3,0),(3,1)\}, & i=2; \\ \{(2,2),(2,3),(3,2),(3,3)\}, & i=3. \end{cases} , \tag{12}$$

as depicted in Fig. 3.

For asymptotically large values of P_M with $q \ll p$ and $r \ll p$, the nonzero probabilities in (11) will tend asymptotically to the following values:

$$\pi_{0,0}\to p^2\ ,\ \pi_{0,1}=\pi_{1,0}\to p(1-p)\ ,\ \pi_{1,1}\to(1-p)^2, \tag{13}$$

in coherence with the asymptotic results reported in [21].

Comparing the approximate distribution in (11) with the asymptotic distribution in (13) highlights on the accuracy of the proposed approximate analysis. In fact, the approximate analysis captures the dependence of the steady-state probabilities, not only on the probability p of the

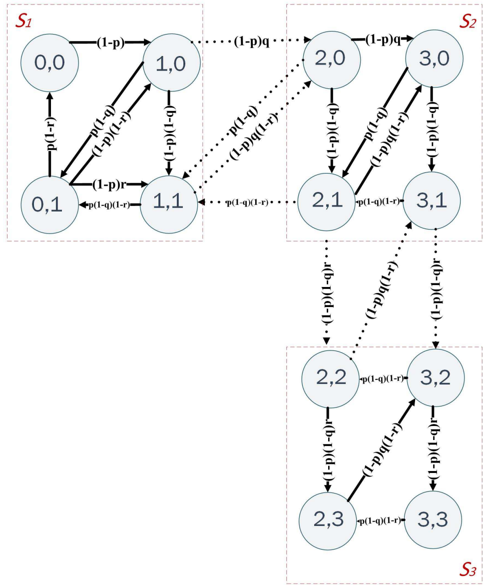

Fig. 3. The closed-set S and its partitioning when hop 1 is the bottleneck.

bottleneck hop, but also on the probabilities q and r of the two remaining hops. The gap between (11) and (13) will increase in the scenarios where q and r are not very small compared to p.

2) Bottleneck Link: Hop 2:

Proposition *2:* If the bottleneck link is hop 2 (i.e. $\max\{p,q,r\}=q$), the steady-state probabilities are given by:

$$\begin{cases} \pi_{L-3,0} &= 0; \\ \pi_{L-3,1} &= \frac{p^2(1-q)}{(p+q+r)(p+q-2pq-pqr+p^2qr)}; \\ \pi_{L-2,0} &= \frac{p^2q(1-p)(1-r)}{(p+q+r)(p+q-2pq-pqr+p^2qr)}; \\ \pi_{L-2,1} &= \frac{pq(1-p)^2}{(p+q+r)(p+q-2pq-pqr+p^2qr)}; \\ \pi_{L-1,0} &= 0; \\ \pi_{L-1,1} &= \frac{q(1-q)}{(p+q(1-q)+r)(1-qr-pq+pqr)}; \\ \pi_{L,0} &= \frac{q^2(1-p)(1-r)}{(p+q(1-q)+r)(1-qr-pq+pqr)}; \\ \pi_{L,1} &= 0; \\ \pi_{L,2} &= \frac{qr^2(1-p)(1-r)}{(p+q+r(1-r))(q+r-2qr+pqr^2-pqr)}; \\ \pi_{L,3} &= 0; \\ \pi_{L-1,2} &= \frac{qr(1-r)^2}{(p+q+r(1-r))(q+r-2qr+pqr^2-pqr)}; \\ \pi_{L-1,3} &= \frac{r^2(1-q)}{(p+q+r(1-r))(q+r-2qr+pqr^2-pqr)}. \end{cases}, \tag{14}$$

while the other probabilities are equal to zero.

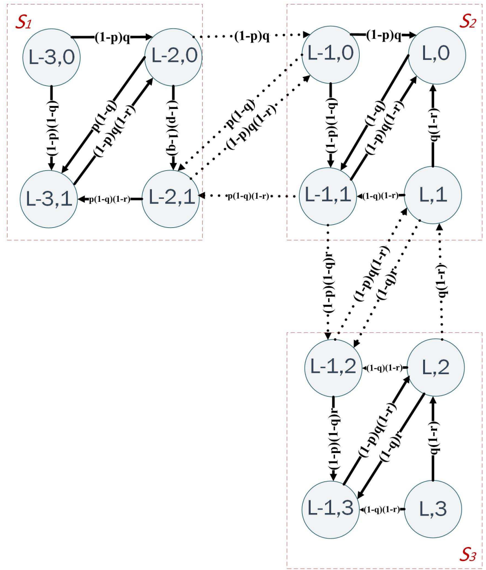

Fig. 4. The closed-set S and its partitioning when hop 2 is the bottleneck.

Proof: The proof is provided in Appendix B. This proof is based on the selection of the subsets S_1, S_2 and S_3 as follows:

$$S_i = \begin{cases} \{(L-3,0),(L-3,1),(L-2,0),(L-2,1)\}\,, & i=1; \\ \{(L-1,0),(L-1,1),(L,0),(L,1)\}\,, & i=2; \\ \{(L-1,2),(L-1,3),(L,2),(L,3)\}\,, & i=3. \end{cases}\,, \qquad (15)$$

where these subsets are shown in Fig. 4.

In coherence with [21], the nonzero asymptotic steady-state probabilities follow from (14) as follows:

$$\pi_{L,0} \to q \quad , \quad \pi_{L-1,1} \to 1-q, \qquad (16)$$

for $p \ll q$ and $r \ll q$.

Similar to the observations made in Section III-B1, the provided approximate analysis relates the steady-state probabilities to the three outage probabilities p, q and r rather than the probability q alone as in (16).

3) Bottleneck Link: Hop 3:

Proposition 3: If the bottleneck link is hop 3 (i.e. $\max\{p,q,r\}=r$), the steady-state probabilities are given by:

$$\begin{cases} \pi_{L-3,L-3} &= \frac{p^3q(1-r)^2}{(p+q+r)c_2}; \\ \pi_{L-3,L-2} &= \frac{p^2r(1-q)(p+r-2pr)}{(p+q+r)c_2}; \\ \pi_{L-2,L-3} &= \frac{p^2qr(1-p)(1-r)}{(p+q+r)c_2}; \\ \pi_{L-2,L-2} &= \frac{pqr^2(1-p)^2}{(p+q+r)c_2}; \\ \pi_{L-1,L-3} &= \frac{q^2(1-p)(1-q)(1-r)^2}{(p+q(1-q)+r)c_3}; \\ \pi_{L-1,L-2} &= \frac{q(1-q)}{(p+q(1-q)+r)c_3}; \\ \pi_{L,L-3} &= \frac{q^2(1-p)(1-r)}{(p+q(1-q)+r)c_3}; \\ \pi_{L,L-2} &= 0; \\ \pi_{L,L-1} &= \frac{r^2(1-p)^2(1-r)}{(p+q+r(1-r))c_4}; \\ \pi_{L,L} &= \frac{r^3(1-p)^2(1-q)}{(p+q+r(1-r))c_4}; \\ \pi_{L-1,L-1} &= \frac{r(1-r)^2}{(p+q+r(1-r))c_4}; \\ \pi_{L-1,L} &= \frac{r^2(1-p)(1-q)(1-r)}{(p+q+r(1-r))c_4}. \end{cases} \tag{17}$$

while the other probabilities are equal to zero. In (17), $c_2=pqr-4pqr^2-4p^2qr+5p^2qr-2p^2r^2+p^2r+pr^2+qr^2+p^2q$, $c_3=1+q-q^2-3qr+2q^2r-2pq+pq^2+3pqr-2pq^2r+qr^2-q^2r^2-pqr^2+pq^2r^2$ and $c_4=1+p^2r+pr^2+qr^2-qr-3pr+pqr^2-p^2qr^2$.

Proof: The proof is provided in Appendix C based on the following selection:

$$S_i=\begin{cases} \{(L-3,L-3),(L-3,L-2),(L-2,L-3), & \\ (L-2,L-2)\}, & i=1; \\ \{(L-1,L-3),(L-1,L-2),(L,L-3), & \\ (L,L-2)\}, & i=2; \\ \{(L-1,L-1),(L-1,L),(L,L-1),(L,L)\}, & i=3. \end{cases}, \tag{18}$$

that is better depicted in Fig. 5.

In coherence with [21], the nonzero probabilities in (17) simplify to the following expressions:

$$\pi_{L,L}\to r^2\ ,\ \pi_{L-1,L}=\pi_{L,L-1}\to r(1-r)\ ,\ \pi_{L-1,L-1}\to(1-r)^2, \tag{19}$$

for $P_M\gg 1$, $p\ll r$ and $q\ll r$.

Similar observations as in Section III-B1 and Section III-B2 can be reached by comparing the approximate and asymptotic steady-state probabilities.

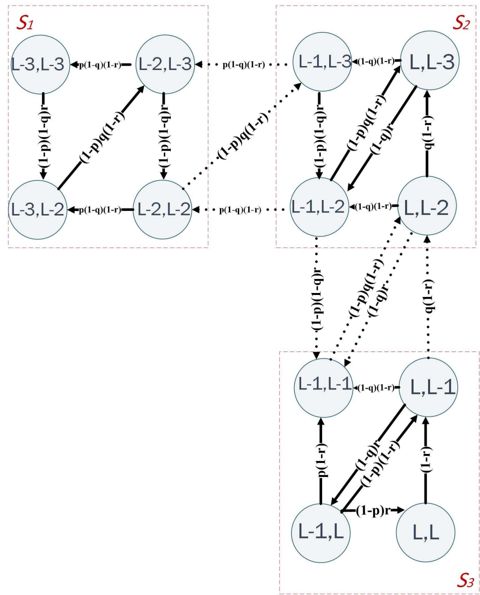

Fig. 5. The closed-set S and its partitioning when hop 3 is the bottleneck.

C. *Outage Probability*

The system will be in outage if no packets can be transmitted along the constituent links [21]. This results from the unavailability of all hops resulting in no change in the occupancy of any of the two buffers. The system outage probability (OP) can be expressed as :

$$P_{out} = \sum_{l,l'} \pi_{l,l'} \Bigg[\left[(1-\delta_{l,L})p + \delta_{l,L}\right] \big[(1-\delta_{l,0})(1-\delta_{l',L})q + \delta_{l,0} + \delta_{l',L} - \delta_{l,0}\delta_{l',L}\big] \left[(1-\delta_{l',0})r + \delta_{l',0}\right] \Bigg], \quad (20)$$

where $\delta_{i,j}$ stands for the Kronecker delta function:

$$\delta_{i,j} = \begin{cases} 1, & i = j; \\ 0, & \text{otherwise.} \end{cases} . \quad (21)$$

The probability multiplying the term $\pi_{l,l'}$ in (20) corresponds to the product of the unavailability probabilities of the three hops. The unavailability of each of the three hops depends on the buffers' states and the FSO channel conditions as follows:

- If the buffer at R_1 is full (i.e. $l = L$ and $\delta_{l,L} = 1$), then no packet can be transmitted along the first hop implying that this hop is unavailable. Otherwise, a packet cannot be transferred on this hop only if it is in outage with probability p.

- If R_1 is empty ($l = 0$) or R_2 is full ($l' = L$), then no packet can traverse the second hop as there is no packet to send, no space for the arriving packet or both. This is captured by the probability $\delta_{l,0} + \delta_{l',L} - \delta_{l,0}\delta_{l',L}$ in (20) that is equal to 1 if either $\delta_{l,0} = 1$ or $\delta_{l',L} = 1$ (or both). Otherwise, $(\delta_{l,0}, \delta_{l',L}) = (0, 0) \Rightarrow (1 - \delta_{l,0})(1 - \delta_{l',L}) = 1$ and the packet cannot traverse the second hop successfully if it is in outage with probability q.
- If the buffer at R_2 is empty (i.e. $l' = 0$ and $\delta_{l',0} = 1$), then no packet can be transmitted along the third hop that becomes unavailable. Otherwise, a packet cannot be transferred on this hop only if it is in outage with probability r.

1) Bottleneck Link: Hop 1: Expanding (20) using the 12 dominant states in (12) results in:

$$\begin{aligned} P_{out} = {} & \pi_{0,0}(p) + \pi_{0,1}(pr) + \pi_{1,0}(pq) + \pi_{1,1}(pqr) + \pi_{2,0}(pq) + \\ & \pi_{2,1}(pqr) + \pi_{3,0}(pq) + \pi_{3,1}(pqr) + pqr(\pi_{2,2} + \pi_{2,3} + \pi_{3,2} + \pi_{3,3}). \end{aligned} \tag{22}$$

Replacing the steady-state probabilities by their values from (11) implies that P_{out} can be written as:

$$\begin{aligned} P_{out} = & \frac{p^4(1-q)(1-r)^2 + p^3 r(1-p)(1-q)(1-r)}{(p+q+r)c} \\ & + \frac{p^3 q(1-p)(1-r)^2 + p^2 qr(1-p)^2}{(p+q+r)c} + \frac{pqr^2}{p+q+r(1-r)} \\ & + \frac{p^2q^2r(1-q) + p^2q^3(1-p)(1-r) + pq^3r(1-p)^2}{(p+q(1-q)+r)(p - pqr + p^2qr + q - 2pq)}. \end{aligned} \tag{23}$$

Since, in this case, $\max\{p, q, r\} = p$:

$$P_{out} \to \frac{p^4}{p} + \frac{0}{p^2} + \frac{0}{p} = p^3. \tag{24}$$

By comparing the OP in (24) with that derived through an asymptotic analysis in [21], we find that both yield the same result. However, the OP expression in (23) reached through the proposed approximate analysis covers more states and, thus, its accuracy is higher.

2) Bottleneck Link: Hop 2: Expanding (20) using the 12 dominant states in (15) results in:

$$\begin{aligned} P_{out} = {} & \pi_{L-3,0}(pq) + \pi_{L-3,1}(pqr) + \pi_{L-2,0}(pq) + \pi_{L-2,1}(pqr) + \pi_{L-1,0}(pq) \\ & + \pi_{L-1,1}(pqr) + \pi_{L,0}(q) + \pi_{L,1}(qr) + \pi_{L-1,2}(pqr) + \pi_{L-1,3}(pqr) + \pi_{L,2}(qr) + \pi_{L,3}(qr). \end{aligned} \tag{25}$$

By further substituting the steady-state probabilities from (14) in (25), P_{out} can be written as:

$$\begin{aligned}P_{out} =& \frac{p^3qr(1-q)+p^3q^2(1-p)(1-r)+p^2q^2r(1-p)^2}{(p+q+r)(p+q-2pq-pqr+p^2qr)}\\&+\frac{pq^2r(1-q)+q^3(1-p)(1-r)}{(p+q(1-q)+r)(1-qr-pq+pqr)}\\&+\frac{pq^2r^2(1-r)^2+pqr^3(1-q)+q^2r^3(1-p)(1-r)}{(p+q+r(1-r))(q+r-2qr+pqr^2-pqr)}.\end{aligned} \tag{26}$$

Since, in this case, $\max\{p,q,r\}=q$:

$$P_{out} \to \frac{0}{q^2}+\frac{q^3}{q}+\frac{0}{q^2}=q^2, \tag{27}$$

that corresponds to the asymptotic value derived in [21]. Evidently, the approximate OP expression in (26) captures the dependence of P_{out} on the three probabilities p, q and r, thus, resulting in better accuracy.

3) Bottleneck Link: Hop 3: Similarly, from (18) and (20):

$$\begin{aligned}P_{out} =& (pqr)(\pi_{L-3,L-3}+\pi_{L-3,L-2}+\pi_{L-2,L-3}+\pi_{L-2,L-2})\\&+\pi_{L-1,L-3}(pqr)+\pi_{L-1,L-2}(pqr)+\pi_{L,L-3}(qr)+\pi_{L,L-2}(qr)\\&+\pi_{L-1,L-1}(pqr)+\pi_{L-1,L}(pr)+\pi_{L,L-1}(qr)+\pi_{L,L}(r),\end{aligned} \tag{28}$$

that, from (17), results in:

$$\begin{aligned}P_{out} =& \frac{pq^3r(1-p)(1-q)(1-r)^2+pq^2r(1-q)}{(p+q(1-q)+r)c_3}+\frac{p^2qr}{p+q+r}\\&+\frac{pq^3r(1-p)(1-r)}{(p+q(1-q)+r)c_3}+\frac{pqr^2(1-r)^2}{(p+q+r(1-r))c_4}+\frac{r^4(1-p)^2(1-q)}{(p+q+r(1-r))c_4}\\&+\frac{pr^3(1-p)(1-q)(1-r)+qr^3(1-p)^2(1-r)}{(p+q+r(1-r))c_4}.\end{aligned} \tag{29}$$

Since, in this case, $\max\{p,q,r\}=r$:

$$P_{out} \to \frac{0}{r}+\frac{0}{r}+\frac{r^4}{r}=r^3. \tag{30}$$

The conclusion, pertaining to the accuracy of the derived OP, is similar to that reached in Section III-C1 and Section III-C2.

D. Average Packet Delay

Storing the information packets in the buffers at R_1 and R_2 results in queuing delays [20]. Following from [21], the average packet delay (APD) of the serial relaying system can be determined from:

$$APD = \left(\frac{1}{\eta_1} - 1\right) + \left(\frac{\bar{L}_1}{\eta_1} + \frac{\bar{L}_2}{\eta_2}\right), \tag{31}$$

where $\bar{L}_n$ and η_n correspond to the average queue length and the effective input throughput at R_n, respectively, for $n = 1, 2$. On the other hand, the term $\frac{1}{\eta_1} - 1$ represents the average delay at S.

The effective throughout at R_n can be computed as follows:

$$\eta_n = \begin{cases} (1-p)(1-\pi_L^{(1)}), & n = 1; \\ (1-q)(1-\pi_0^{(1)})(1-\pi_L^{(2)}), & n = 2, \end{cases}, \tag{32}$$

where $\pi_l^{(n)}$ denotes the steady-state probability of having l packets in R_n's buffer. Equation (32) highlights that a packet will enter the buffer at R_1 only if this buffer is not full and the S-R_1 link is not in outage. Similarly, a packet will enter the buffer at R_2 only if (i): the previous buffer at R_1 is not empty, (ii): the buffer at R_2 is not full and (iii): the link R_1-R_2 is not in outage.

The marginal probabilities $\{\pi_l^{(1)}, \pi_l^{(2)}\}_{l=0}^{L}$ in (32) can be calculated from $\pi_l^{(1)} = \sum_{l'=0}^{L} \pi_{l,l'}$ and $\pi_{l'}^{(2)} = \sum_{l=0}^{L} \pi_{l,l'}$. Following from these probabilities, the average queue lengths in (31) can be derived from:

$$\bar{L}_n = \sum_{l=0}^{L} l\pi_l^{(n)} = \begin{cases} \sum_{l=0}^{L}\sum_{l'=0}^{L} l\pi_{l,l'}, & n = 1; \\ \sum_{l=0}^{L}\sum_{l'=0}^{L} l'\pi_{l,l'}, & n = 2. \end{cases} \tag{33}$$

Finally, replacing the steady-state probabilities from (11), (14) or (17) in (32) and (33) results in the approximate APD expressions that turn out to be very accurate in the average-to-high SNR range. This improved accuracy results from covering more states in the approximate analysis as compared to [21].

1) Bottleneck Link: Hop 1: In the case where $\max\{p, q, r\} = p$, the steady-state probabilities in (11) tend to the following asymptotic values:

$$\begin{cases} \pi_{0,0} \to \frac{p^3}{p} = p^2, & \pi_{2,0} = 0, & \pi_{2,2} \to 0, \\ \pi_{0,1} \to \frac{p^2}{p} = p, & \pi_{2,1} \to 0, & \pi_{2,3} \to 0, \\ \pi_{1,0} \to \frac{p^2}{p} = p, & \pi_{3,0} \to 0, & \pi_{3,2} \to 0, \\ \pi_{1,1} \to \frac{p}{p} = 1, & \pi_{3,1} \to 0, & \pi_{2,3} \to 0; \end{cases}. \tag{34}$$

As shown in (34), $\pi_{1,1} \to 1$ indicating that, at steady-state, both buffers will most probably contain one packet ($\bar{L}_n \to 1$ for $n = 1, 2$). This is in accordance with the fact that the poor quality of the first hop will reduce the input throughputs to both relays that are placed in series. Accordingly, from (32), both η_1 and η_2 will tend to 1 since the probability of obtaining empty or full buffers tends to 0 . This will result in an APD value tending to 2.

2) Bottleneck Link: Hop 2: In the case where $\max\{p, q, r\} = q$, following from (14):

$$\begin{cases} \pi_{L-3,0} = 0, & \pi_{L-1,0} = 0, & \pi_{L-1,2} \to 0, \\ \pi_{L-3,1} \to 0, & \pi_{L-1,1} \to \frac{q}{q} = 1, & \pi_{L-1,3} \to 0, \\ \pi_{L-2,0} \to 0, & \pi_{L,0} \to 0, & \pi_{L,2} \to 0, \\ \pi_{L-3,1} \to 0, & \pi_{L,1} = 0, & \pi_{L,3} = 0; \end{cases} . \tag{35}$$

As shown in (35), $\pi_{L-1,1} \to 1$ indicating that, at steady-state, $\bar{L}_1 \to L - 1$ and $\bar{L}_2 \to 1$. This is in accordance with the fact that the flow of packets will occur more efficiently along the S-R$_1$ and R$_2$-D hops than along the bottleneck link R$_1$-R$_2$. This will result in filling the buffer at R$_1$ at a faster pace compared to the buffer at R$_2$. From (32), both η_1 and η_2 will tend to 1. This will result in an APD value tending to L following from (31).

3) Bottleneck Link: Hop 3: In the case where $\max\{p, q, r\} = r$, following from (17):

$$\begin{cases} \pi_{L-3,L-3} \to 0, & \pi_{L-1,L-3} \to 0, & \pi_{L-1,L-1} \to \frac{r}{r} = 1, \\ \pi_{L-3,L-2} \to 0, & \pi_{L-1,L-2} \to 0, & \pi_{L-1,L} \to \frac{r^2}{r} = r, \\ \pi_{L-2,L-3} \to 0, & \pi_{L,L-3} \to 0, & \pi_{L,L-1} \to \frac{r^2}{r} = r, \\ \pi_{L-3,L-2} \to 0, & \pi_{L,L-2} = 0, & \pi_{L,L} \to \frac{r^3}{r} = r^2; \end{cases} . \tag{36}$$

As observed in (36), $\pi_{L-1,L-1} \to 1$ indicating that, at steady-state, $\bar{L}_1 \to L-1$ and $\bar{L}_2 \to L-1$. This is due to the minimal output throughput at R_2 that will result in the congestion of the buffers. As in Section III-D1 and Section III-D2, both η_1 and η_2 will tend to 1 following from (32). This will result in an APD value tending to $2(L-1)$.

IV. Numerical Results

We next report some numerical results that support the aforementioned findings reported in the preceding sections. As previously mentioned in Section II, R_1 and R_2 are situated serially between S and D and their positions are determined by the vector $\mathbf{d} = (d_1, d_2, d_3)$ with $d_{SD} = \sum_{n=1}^{3} d_n$ (where all distances are expressed in km). The refractive index structure parameter and the attenuation constant are set to be $C_n^2 = 1.7\text{x}10^{-14}$ m$^{-2/3}$ and $\sigma = 0.44$ dB/km, respectively.

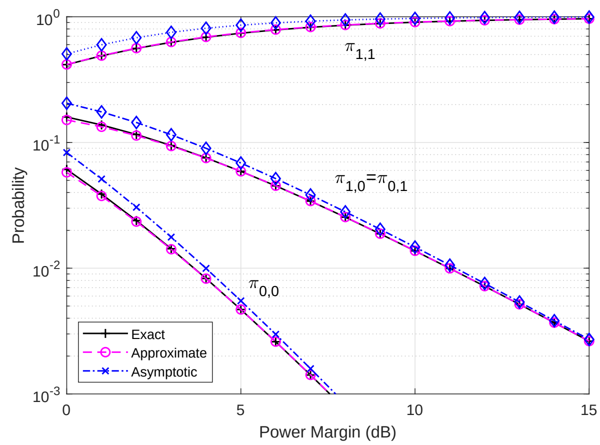

Fig. 6. Dominant group of steady-state probabilities for $\mathbf{d} = (3, 2, 2)$ km.

We also assume an operating wavelength λ of 1550 nm, a total distance d_{SD} of 7 km, and a buffer size L of 5. In what follows, as a benchmark, we also show the asymptotic results derived in [21]. The receiver radius, beam waist and pointing error displacement standard deviation are assumed to be the same for all hops and they will be denoted by a, ω_z, and σ_s, respectively. In what follows, we set $\sigma_s/a = 3$ and $\omega_z/a = 25$.

As a benchmark, we show the performance of the 3-hop buffer-free (BF) system. This system will not suffer from outage only if the three constituent hops are not in outage resulting in $P_{out} = 1 - (1-p)(1-q)(1-r)$. We also show the performance of the 2-hop BF and BA systems [21]. For these systems, we assume that the relay is placed at the distance $d_1 + d_2/2$ from S and at the distance $d_3 + d_2/2$ from D thus maintaining the same end-to-end distance of $d_{SD} = \sum_{n=1}^{3} d_n$. Finally, we show the performance of the 1-hop system where S and D communicate directly over a link of distance d_{SD}.

Fig. 6, Fig. 7 and Fig. 8 show the performance with $\mathbf{d} = (3, 2, 2)$ km, where hop 1 is the bottleneck. As predicted in (13), for large values of P_M, the probability is mostly split among the states $\mathbf{l} = (0, 0)$, $\mathbf{l} = (1, 0)$, $\mathbf{l} = (0, 1)$, and $\mathbf{l} = (1, 1)$. In this simulation setup, $\pi_{0,1} = \pi_{1,0}$ following from (11) since $q = r$ following from the fact that $d_2 = d_3$. The steady-state probabilities of these dominant states are plotted as a function of P_M in Fig. 6. Results in Fig. 6 highlight on the high accuracy of the probabilities derived in (11) over the entire range of values of P_M. In fact, the approximate curves practically overlap with the exact curves for P_M values as small as 0 dB. Regarding the asymptotic steady-state probabilities from [21], while

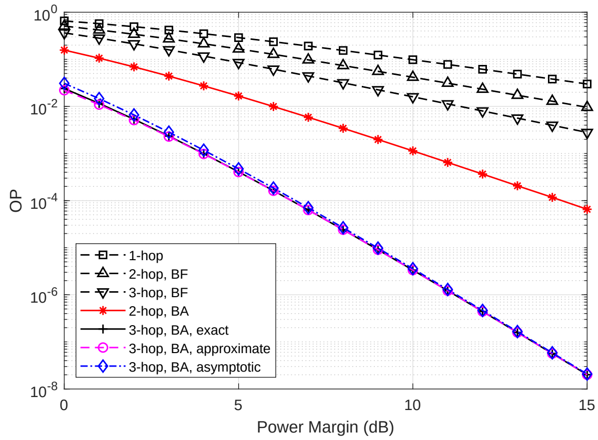

Fig. 7. OP for $\mathbf{d} = (3, 2, 2)$ km.

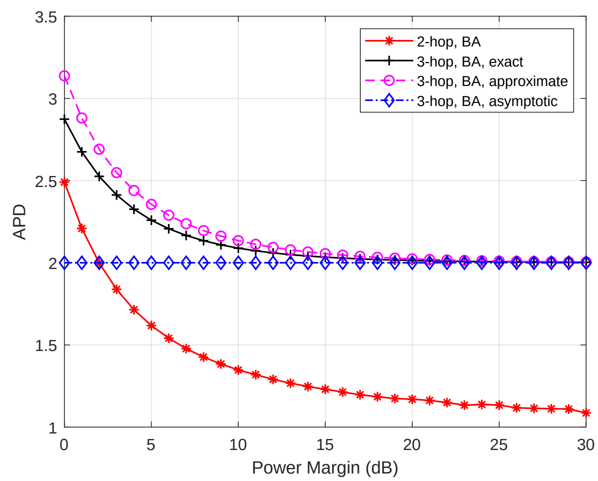

Fig. 8. APD for $\mathbf{d} = (3, 2, 2)$ km.

the asymptotic values of $\pi_{0,0}$, $\pi_{1,0}$ and $\pi_{0,1}$ show close match with the exact ones for the values of P_M exceeding 10 dB, this accuracy is compromised for the largest probability $\pi_{1,1}$ where the gap is noticeable for values of P_M up to 15 dB. Regarding OP, in Fig. 7, the approximate and exact OP curves almost perfectly overlap with each other for all values of P_M. In terms of APD, Fig. 8 reveals that in comparison to the results obtained by the asymptotic analysis, the approximate analysis yields results much closer to the exact APD for all P_M values. Results in Fig. 7 show that equipping the relays with buffers results in significant reductions in the OP. Moreover, increasing the number of relays from 1 to 2 reduces the OP even for the same value of

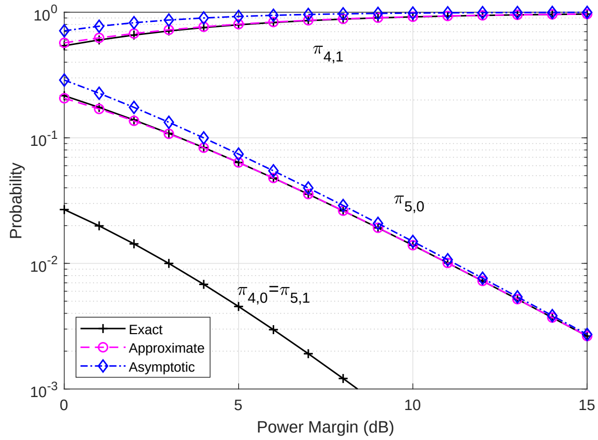

Fig. 9. Dominant group of steady-state probabilities for $\mathbf{d} = (2, 3, 2)$ km. The approximate and asymptotic values of $\pi_{4,0}$ and $\pi_{5,1}$ are equal to zero following from (14) and (16).

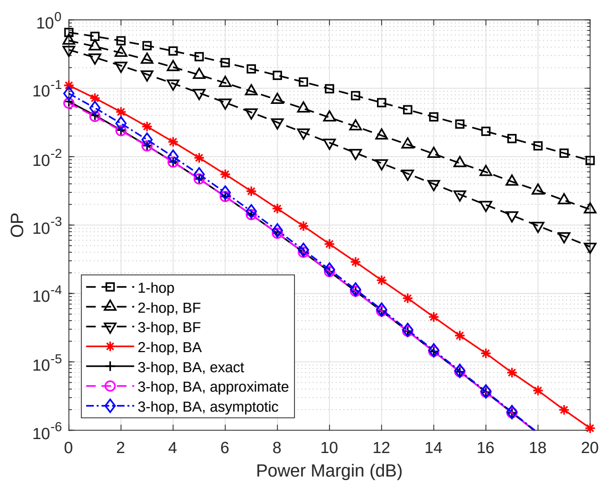

Fig. 10. OP for $\mathbf{d} = (2, 3, 2)$ km.

the total distance d_{SD}. For example, at an OP value of 10^{-4}, the 3-hop BA system outperforms the 2-hop BA system by around 7.8 dB. This reduction in the OP is associated with an increase in the APD as shown in Fig. 8 since the packets will be queued at one additional buffer before reaching the destination.

Fig. 9, Fig. 10 and Fig. 11 illustrate the performance with hop 2 as the bottleneck hop for $\mathbf{d} = (2, 3, 2)$ km. As expected from (16), the dominant state is clearly observed to be $\mathbf{l} = (L - 1, 1) = (4, 1)$ followed by the state $\mathbf{l} = (L, 0) = (5, 0)$ as highlighted in Fig. 9.

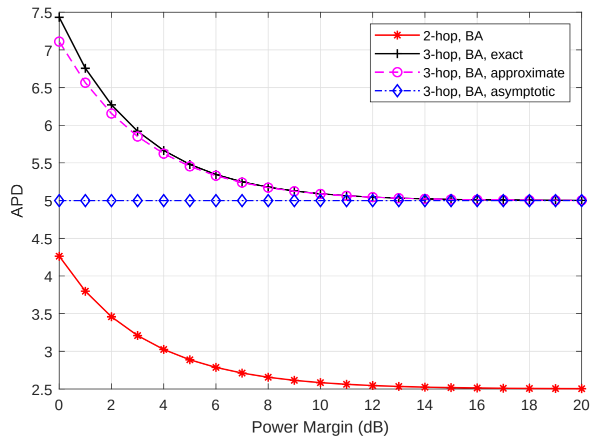

Fig. 11. APD for $\mathbf{d} = (2, 3, 2)$ km.

A shown in this figure, the gap between the approximate and exact values of $\pi_{4,1}$ and $\pi_{5,0}$ is practically negligible for all values of P_M. Regarding the remaining states $(4, 0)$ and $(5, 1)$, both (14) and (16) predicted that the corresponding approximate and asymptotic steady-state probabilities are zero. This prediction is not problematic since the exact probabilities $\pi_{4,0}$ and $\pi_{5,1}$ are several orders of magnitude smaller than the probabilities $\pi_{4,1}$ and $\pi_{5,0}$ as shown in Fig. 9. Comparing the OP curves in Fig. 10 yields to similar findings as in Fig. 7 where the exact and approximate OP curves practically overlap with each other for all values of P_M. Moreover, as in Fig. 7, the gap between the asymptotic and exact OP curves is insignificant for average-to-large values of P_M. In terms of APD, Fig. 11 reveals that the approximate analysis yields results close to the exact APD where the two corresponding curves overlap with each other for $P_M \geq 6$ dB. Whereas, the asymptotic APD shows significant deviation from both the exact and approximate APD curves for low P_M values. Results in Fig. 10 and Fig. 11 show that the 3-hop BA system achieves the smallest OP at the expense of increasing the APD. Results in Fig. 10 also highlight on the benefit of placing two relays between S and D. For example, at an OP value of 10^{-2}, the 3-hop system outperforms the 1-hop system by 9 dB and 16 dB in the absence and presence of buffers, respectively.

Fig. 12, Fig. 13 and Fig. 14 show the performance for the third scenario where hop 3 is the bottleneck with $\mathbf{d} = (2, 2, 3)$ km. From (19), the probability is split, as observed in Fig. 12, among the states $\mathbf{l} = (L-1, L-1) = (4, 4)$, $\mathbf{l} = (L-1, L) = (4, 5)$, $\mathbf{l} = (L, L-1) = (5, 4)$, and $\mathbf{l} = (L, L) = (5, 5)$. In this simulation setup, $\pi_{4,5} = \pi_{5,4}$ following from (17) since

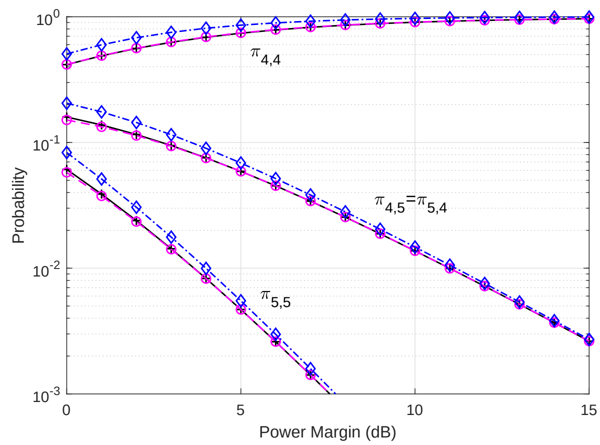

Fig. 12. Dominant group of steady-state probabilities for $\mathbf{d} = (2, 2, 3)$ km.

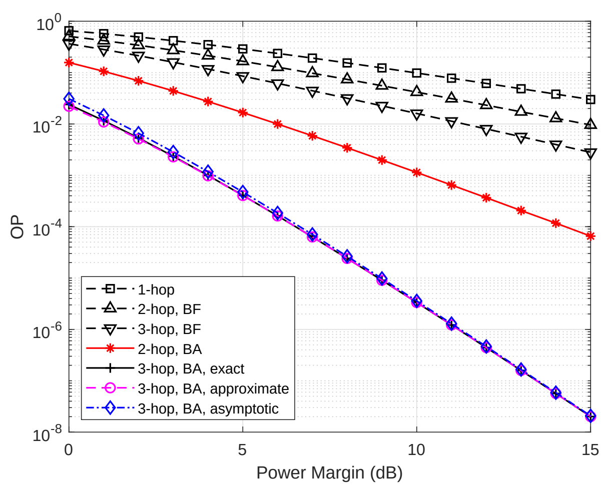

Fig. 13. OP for $\mathbf{d} = (2, 2, 3)$ km.

$p = q$ following from the fact that $d_1 = d_2$. Figures 12, 13 and 14 demonstrate the accuracy of the proposed performance evaluation approach in this third scenario as well. Regarding the asymptotic approach in [21], while the asymptotic OP manifests an acceptable level of accuracy as shown in Fig. 13, the asymptotic APD value of $2(L-1) = 8$ diverges significantly from the exact APD for P_M values below 10 dB as highlighted in Fig. 14. This further stresses on the significance of the presented approximate analysis. Results in Fig. 13 demonstrate the boosted levels of reliability that can be reaped from equipping the relays with buffers. For example, at an OP value of 10^{-2}, the BA systems outperform the BF systems by 9 dB and 10 dB with one

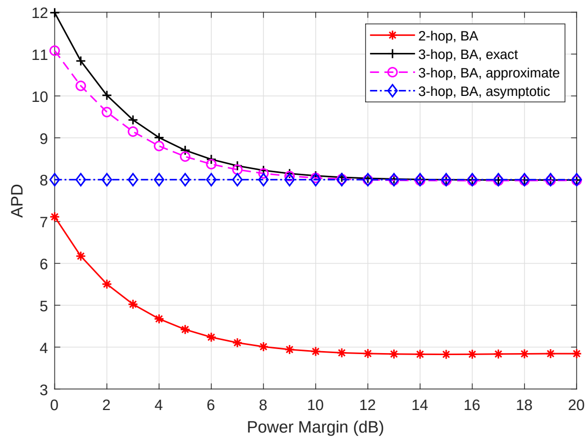

Fig. 14. APD for $\mathbf{d} = (2, 2, 3)$ km.

relay and two relays, respectively.

V. Conclusion

In this paper, we studied a three-hop BA FSO system where three different cases arose depending on the bottleneck hop. For each case, we derived the outage probability and average packet delay through an approximate analysis as exact solutions have seemed to be out of reach due to the large number of states. Results confirm that the adopted methodology results in OP and APD of higher accuracy than those reached using an asymptotic analysis.

Appendix A

The inter-subset transition probabilities are presented by the dotted arrows in Fig. 3. From (9), since x, y and z stand for the steady-state probabilities of being in subsets S_1, S_2 and S_3, respectively, then the balance equations between the subsets can be written as: $[(1-p)q]x = [p(1-q)]y$ and $[(1-p)(1-q)r]y = [(1-p)q(1-r)]z$. Solving these equations along with the equation $x + y + z = 1$ results in:

$$x = \frac{p}{p+q+r} \tag{37}$$

$$y = \frac{q}{p+q(1-q)+r} \tag{38}$$

$$z = \frac{r}{p+q+r(1-r)}. \tag{39}$$

Next, we derive the balance equations pertaining to the subset S_1 by assuming that it is closed.

At $\mathbf{l} = (0,0)$: $(1-p)\pi_{0,0} = p(1-r)\pi_{0,1} \implies \pi_{0,1} = \frac{1-p}{p(1-r)}\pi_{0,0}$.

At $\mathbf{l} = (1,0)$, the transition probability $t_{(1,0),(2,0)}$ will be neglected as this transition is not confined in S_1. Therefore, the approximate balance equation becomes: $(1-q)\pi_{1,0} = (1-p)\pi_{0,0} + (1-p)(1-r)\pi_{0,1} = (1-p)\pi_{0,0} + (1-p)(1-r)\frac{1-p}{p(1-r)}\pi_{0,0} = (1-p)\pi_{0,0}(1+\frac{1-p}{p}) \implies \pi_{1,0} = \frac{1-p}{(1-q)p}\pi_{0,0}$.

At $\mathbf{l} = (1,1)$, the probabilities $t_{(1,1),(2,0)}$, $t_{(1,1),(1,2)}$, $t_{(2,1),(1,1)}$, $t_{(2,0),(1,1)}$ and $t_{(0,2),(1,1)}$ will be neglected as these transitions are not confined in S_1. Consequently, the approximate balance equation can be written as: $p(1-q)(1-r)\pi_{1,1} = (1-p)r\pi_{0,1} + (1-p)(1-q)\pi_{1,0} = \left[\frac{(1-p)^2 r}{p(1-r)} + \frac{(1-p)^2}{p}\right]\pi_{0,0} = \frac{(1-p)^2}{p}\left[\frac{r}{1-r}+1\right]\pi_{0,0} \implies \pi_{1,1} = \frac{(1-p)^2}{p^2(1-q)(1-r)^2}\pi_{0,0}$.

Therefore, the following relations hold:

$$\begin{cases} \pi_{0,1} &= \frac{1-p}{p(1-r)}\pi_{0,0}; \\ \pi_{1,0} &= \frac{1-p}{(1-q)p}\pi_{0,0}; \\ \pi_{1,1} &= \frac{(1-p)^2}{p^2(1-q)(1-r)^2}\pi_{0,0}. \end{cases} . \tag{40}$$

Since $\pi_{0,0} + \pi_{0,1} + \pi_{1,0} + \pi_{1,1} = x$, then the following relation follows from (37) and (40):

$$\pi_{0,0}\left(1 + \frac{1-p}{p(1-r)} + \frac{1-p}{(1-q)p} + \frac{(1-p)^2}{p^2(1-q)(1-r)^2}\right) = \frac{p}{p+q+r}. \tag{41}$$

Simplifying the above equation and replacing in (40) result in the first four equations provided in (11).

Next, we consider the transitions inside S_2. At $\mathbf{l} = (2,0)$, all transition probabilities of the form $t_{(2,0),\mathbf{l}'}$ are neglected as $\mathbf{l}' \notin S_2$ implying that $\pi_{2,0} = 0$.

At $\mathbf{l} = (3,0)$, the probability $t_{(3,0),(4,0)}$ will be neglected as the transition is not limited in S_2 and the balance equation becomes: $(1-q)\pi_{3,0} = (1-p)q(1-r)\pi_{2,1} \implies \pi_{3,0} = \frac{(1-p)q(1-r)}{1-q}\pi_{2,1}$.

At $\mathbf{l} = (3,1)$, the probabilities $t_{(3,1),(4,0)}$, $t_{(3,1),(3,2)}$, $t_{(4,0),(3,1)}$, $t_{(4,1),(3,1)}$ and $t_{(2,2),(3,1)}$ will all tend to zero as the transitions are not limited in S_2 and the balance equation becomes: $p(1-q)(1-r)\pi_{3,1} = (1-p)(1-q)\pi_{3,0} = q(1-r)(1-p)^2\pi_{2,1} \implies \pi_{3,1} = \frac{(1-p)^2 q}{p(1-q)}\pi_{2,1}$.

Therefore, the following relations hold:

$$\begin{cases} \pi_{2,0} &= 0; \\ \pi_{3,0} &= \frac{(1-p)q(1-r)}{1-q}\pi_{2,1}; \\ \pi_{3,1} &= \frac{(1-p)^2 q}{p(1-q)}\pi_{2,1}. \end{cases} . \tag{42}$$

Since $\pi_{2,0} + \pi_{2,1} + \pi_{3,0} + \pi_{3,1} = y$, then from (38) and (42):

$$\pi_{2,1}\left(1 + \frac{(1-p)q(1-r)}{1-q} + \frac{(1-p)^2 q}{p(1-q)}\right) = \frac{q}{p+q(1-q)+r}. \tag{43}$$

Simplifying the above equation and replacing in (42) result in the second set of four equations in (11).

Finally, we consider the subset S_3. At $\mathbf{l} = (2,2)$, neglecting the probabilities unconfined to S_3 yields: $(1-p)(1-q)r\pi_{2,2} = p(1-q)(1-r)\pi_{3,2} \implies \pi_{2,2} = \frac{p(1-r)}{(1-p)r}\pi_{3,2}$. At $\mathbf{l} = (2,3)$: $(1-p)q(1-r)\pi_{2,3} = (1-q)\left[p(1-r)+r(1-p)\right]\pi_{3,2} \implies \pi_{2,3} = \frac{1-q}{q}\left[\frac{p}{1-p}+\frac{r}{1-r}\right]\pi_{3,2}$. At $\mathbf{l} = (3,3)$: $p(1-q)(1-r)\pi_{3,3} = (1-p)(1-q)r\pi_{3,2} \implies \pi_{3,3} = \frac{(1-p)r}{p(1-r)}\pi_{3,2}$.

Therefore, the following relations hold:

$$\begin{cases} \pi_{2,2} &= \frac{p(1-r)}{(1-p)r}\pi_{3,2}; \\ \pi_{2,3} &= \frac{1-q}{q}\left[\frac{p}{1-p}+\frac{r}{1-r}\right]\pi_{3,2}; \\ \pi_{3,3} &= \frac{(1-p)r}{p(1-r)}\pi_{3,2}. \end{cases} \quad . \tag{44}$$

Since $\pi_{2,2}+\pi_{2,3}+\pi_{3,2}+\pi_{3,3} = z$, then from (39) and (44):

$$\pi_{3,2}\left(1+\frac{p(1-r)}{(1-p)r}+\frac{1-q}{q}\left[\frac{p}{1-p}+\frac{r}{1-r}\right]+\frac{(1-p)r}{p(1-r)}\right) = \frac{r}{p+q+r(1-r)}. \tag{45}$$

Simplifying the above equation and replacing in (44) result in the last four equations in (11).

Appendix B

Similar to Appendix A, we will first consider the inter-subset transition probabilities denoted by the dotted arrows in Fig. 4. Solving the two corresponding balance equations:

$$y = \frac{(1-p)q}{p(1-q)}x \quad ; \quad z = \frac{(1-q)r}{q(1-r)}y, \tag{46}$$

as well as the equation $x+y+z=1$ results in:

$$x = \frac{p}{p+q+r} \tag{47}$$

$$y = \frac{q}{p+q(1-q)+r} \tag{48}$$

$$z = \frac{r}{p+q+r(1-r)}. \tag{49}$$

It is worth highlighting that in developing (46), the transition probability $\pi_{(L-2,1),(L-1,0)} = (1-p)q(1-r)$ was approximated by $(1-p)q$ so that $\pi_{(L-2,1),(L-1,0)} \approx \pi_{(L-2,0),(L-1)} = (1-p)q$ that will denote the inter-subset transition probability from subset S_1 to subset S_2. Similar approximations are used to determine the transition probabilities from $S_2 \to S_1$, $S_2 \to S_3$ and $S_3 \to S_2$.

Looking into S_1, we solve the three following balance equations where we neglect all the transitions to or from a state outside the set S_1. (i): At $\mathbf{l} = (L-3,0)$, $\pi_{L-3,0} = 0$. (ii): At

$\mathbf{l} = (L-2,0)$, $(1-p)(1-q)\pi_{L-2,0} = p(1-q)(1-r)\pi_{L-2,1} \implies \pi_{L-2,0} = \frac{p(1-r)}{1-p}\pi_{L-2,1}$.
(ii): At $\mathbf{l} = (L-3,1)$, $(1-p)q(1-r)\pi_{L-3,1} = p(1-q)(1-r)\pi_{L-2,1} + p(1-q)\pi_{L-2,0} = \left[p(1-q)(1-r) + \frac{p^2(1-q)(1-r)}{1-p}\right]\pi_{L-2,1} \implies \pi_{L-3,1} = \frac{p(1-q)}{(1-p)^2 q}\pi_{L-2,1}$.

Therefore, the following relations hold:

$$\begin{cases} \pi_{L-3,0} &= 0; \\ \pi_{L-2,0} &= \frac{(1-p)q(1-r)}{(1-q)}\pi_{L-3,1}; \\ \pi_{L-2,1} &= \frac{(1-p)^2 q}{p(1-q)}\pi_{L-3,1}. \end{cases} \tag{50}$$

Solving (50) while taking into consideration that $\pi_{L-3,0}+\pi_{L-3,1}+\pi_{L-2,0}+\pi_{L-2,1} = x$ results in:

$$\pi_{L-3,1}\left(1 + \frac{(1-p)q(1-r)}{(1-q)} + \frac{(1-p)^2 q}{p(1-q)}\right) = \frac{p}{p+q+r}, \tag{51}$$

where the probability x was replaced by its value from (47). Finally, replacing (51) in (50) results in the first four equations in (14).

Next, consider S_2. At $\mathbf{l} = (L-1,0)$ and $\mathbf{l} = (L,1)$, all transition probabilities are neglected as all the transitions to these states are from states outside of this set implying that $\pi_{L-1,0} = 0$ and $\pi_{L,1} = 0$. At $\mathbf{l} = (L,0)$: $(1-q)\pi_{L,0} = \frac{(1-p)q(1-r)}{1-q}\pi_{L-1,1}$. Combining this equation along with the equation $\pi_{L-1,0}+\pi_{L-1,1}+\pi_{L,0}+\pi_{L,1} = \pi_{L-1,1}+\pi_{L,0} = y$ results in the second set of four equations in (14) where y is replaced by its value from (48).

In regards to the third subset S_3, at $\mathbf{l} = (L,3)$, $\pi_{L,3} = 0$. At $\mathbf{l} = (L-1,2)$: $(1-p)(1-q)r\pi_{L-1,2} = (1-q)(1-r)\pi_{L,2} \implies \pi_{L-1,2} = \frac{1-r}{(1-p)r}\pi_{L,2}$. At $\mathbf{l} = (L-1,3)$: $(1-p)q(1-r)\pi_{L-1,3} = (1-q)\left(r+(1-r)\right)r\pi_{3,2} \implies \pi_{L-1,3} = \frac{1-q}{(1-p)q(1-r)}\pi_{L,2}$. Combining these relations results in:

$$\begin{cases} \pi_{L,3} &= 0; \\ \pi_{L-1,2} &= \frac{1-r}{(1-p)r}\pi_{L,2}; \\ \pi_{L-1,3} &= \frac{1-q}{(1-p)q(1-r)}\pi_{L,2}. \end{cases} . \tag{52}$$

Since $\pi_{L,2}+\pi_{L,3}+\pi_{L-1,2}+\pi_{L-1,3} = z = \frac{r}{p+q+r(1-r)}$ from (49), then solving (52) results in:

$$\pi_{L,2}\left(1 + \frac{1-r}{(1-p)r} + \frac{1-q}{(1-p)q(1-r)}\right) = \frac{r}{p+q+r(1-r)}. \tag{53}$$

Finally (52) and (53) result in the last set of four relations in (14).

Appendix C

Similar to the previous appendices, solving the inter-subset balance equations along with $x+y+z=1$ results in (refer to Fig. 5):

$$x = \frac{p}{p+q+r} \tag{54}$$

$$y = \frac{q}{p+q(1-q)+r} \tag{55}$$

$$z = \frac{r}{p+q+r(1-r)}. \tag{56}$$

Looking into S_1, similar derivation steps as those provided in Appendix A and Appendix B show that the local balance equations will result in:

$$\begin{cases} \pi_{L-3,L-3} & = \frac{p(1-r)}{(1-p)r}\pi_{L-2,L-3}; \\ \pi_{L-2,L-2} & = \frac{(1-p)r}{p(1-r)}\pi_{L-2,L-3}; \\ \pi_{L-3,L-2} & = \frac{1-q}{q}\left[\frac{p}{1-p}+\frac{r}{1-r}\right]\pi_{L-2,L-3}. \end{cases}, \tag{57}$$

implying that:

$$\pi_{L-2,L-3}\left(1+\frac{p(1-r)}{(1-p)r}+\frac{(1-p)r}{p(1-r)}+\frac{1-q}{q}\left[\frac{p}{1-p}+\frac{r}{1-r}\right]\right) = \frac{p}{p+q+r}, \tag{58}$$

since $\pi_{L-3,L-3}+\pi_{L-3,L-2}+\pi_{L-2,L-3}+\pi_{L-2,L-2}=x$.

At S_2, the balance equations will yield the following relations:

$$\begin{cases} \pi_{L,L-2} & = 0; \\ \pi_{L-1,L-3} & = \frac{(1-q)(1-r)}{(1-p)(1-q)r}\pi_{L,L-3}; \\ \pi_{L-1,L-2} & = \frac{1-q}{(1-p)q(1-r)}\pi_{L,L-3}. \end{cases}. \tag{59}$$

Solving (59) along with the relation $\pi_{L-1,L-3}+\pi_{L-1,L-2}+\pi_{L,L-3}+\pi_{L,L-2}=y$ results in:

$$\pi_{L,L-3}\left(1+(1-q)(1-r)+\frac{1-q}{(1-p)q(1-r)}\right) = \frac{q}{p+q(1-q)+r}. \tag{60}$$

In regards to the third subset S_3, the following relations hold:

$$\begin{cases} \pi_{L-1,L} & = \frac{1-r}{(1-p)r}\pi_{L,L}; \\ \pi_{L,L-1} & = \frac{1-r}{(1-q)r}\pi_{L,L}; \\ \pi_{L-1,L-1} & = \frac{(1-r)^2}{(1-p)^2(1-q)r^2}\pi_{L,L}. \end{cases}. \tag{61}$$

Since $\pi_{L,L-1}+\pi_{L,L}+\pi_{L-1,L-1}+\pi_{L-1,L}=z$, then (56) and (61) yield:

$$\pi_{L,L}\left(1+\frac{1-r}{(1-p)r}+\frac{1-r}{(1-q)r}+\frac{(1-r)^2}{(1-p)^2(1-q)r^2}\right) = \frac{r}{p+q+r(1-r)}. \tag{62}$$

Finally, replacing (58), (60) and (62) in (57), (59) and (61), respectively, results in the solution provided in (17).

REFERENCES

[1] N. Nomikos, T. Charalambous, I. Krikidis, D. N. Skoutas, D. Vouyioukas, M. Johansson, C. Skianis, A survey on buffer-aided relay selection, IEEE Comm. Surveys Tutorials 18 (2) (2016) 1073–1097.

[2] Y. Zhang, Y. Park, B. Kim, K. Kim, Performance analysis of hybrid FSO/RF system, in: Proc of Int. Conf. on Ubiquitous and Future Networks (2011) 279–283.

[3] M. A. Khalighi, M. Uysal, Survey on free space optical communication: A communication theory perspective, IEEE Comm. Surveys Tutorials, 16 (4) (2014) 2231–2258.

[4] N. D. Chatzidiamantis, D. S. Michalopoulos, E. E. Kriezis, G. K. Karagiannidis, R. Schober, Relay selection in relay-assisted free space optical systems, in: Proc. IEEE Global Telecomm. Conf. (2011) 1–6.

[5] L. Yang, X. Gao, M. S. Alouini, Performance analysis of relay-assisted all-optical FSO networks over strong atmospheric turbulence channels with pointing errors, IEEE/OSA J. Lightwave Technol. 32 (23) (2014), 4613–4620.

[6] C. Abou-Rjeily, Z. Noun, Impact of inter-relay cooperation on the performance of FSO systems with any number of relays, IEEE Trans. Wireless Commun. 15 (6) (2016) 3796–3809.

[7] N. Zlatanov, A. Ikhlef, T. Islam, R. Schober, Buffer-aided cooperative communications: Opportunities and challenges, IEEE Commun. Mag. 52 (4) (2014) 146–153.

[8] M. Karimi, M. Nasiri-Kenari, Free-space optical communications via optical amplify-and-forward relaying, IEEE/OSA J. Lightwave Technol. 29 (2) (2011) 242–248.

[9] B. Zhu, J. Cheng, M. Alouini, L. Wu, Relay placement for FSO multi-hop DF systems with link obstacles and infeasible regions, IEEE Trans. Wireless Commun. 14 (9) (2015) 5240–5250.

[10] C. Abou-Rjeily, A. Abdo, Serial relaying over gamma-gamma MIMO FSO links: Diversity order and aperture allocation, IEEE Commun. Lett. 19 (4) (2015) 553–556.

[11] M. Safari, M. Uysal, Relay-assisted free-space optical communication, IEEE Trans. Wireless Commun. 7 (12) (2008) 5441–5449.

[12] C. Abou-Rjeily, Achievable diversity orders of decode-and-forward cooperative protocols over gamma-gamma fading FSO links, IEEE Trans. Commun. 61 (9) (2013) 3919–3930.

[13] A. Ikhlef, D. S. Michalopoulos, R. Schober, Buffers improve the performance of relay selection, in: Proc. IEEE Global Telecomm. Conf. (2011) 1–6.

[14] I. Krikidis, T. Charalambous, J. S. Thompson, Buffer-aided relay selection for cooperative diversity systems without delay constraints, IEEE Trans. Wireless Commun. 11 (5) (2012) 1957–1967.

[15] Z. Tian, Y. Gong, G. Chen, J. Chambers, Buffer-aided relay selection with reduced packet delay in cooperative networks, IEEE Trans. Veh. Technol. 66 (3) (2017) 2567–2575.

[16] B. Manoj, R. K. Mallik, M. R. Bhatnagar, Performance analysis of buffer-aided priority-based max-link relay selection in DF cooperative networks, IEEE Trans. Commun. 66 (7) (2018) 2826–2839.

[17] Z. Tian, G. Chen, Y. Gong, Z. Chen, J. A. Chambers, Buffer-aided max-link relay selection in amplify-and-forward cooperative networks, IEEE Trans. Veh. Technol. 64 (2) (2015) 553–565.

[18] Y. F. Al-Eryani, A. M. Salhab, S. A. Zummo, M. S. Alouini, Protocol design and performance analysis of multiuser mixed RF and hybrid FSO/RF relaying with buffers. IEEE/OSA Journal of Optical Comm. and Netw. 10 (4) (2018) 309–321.

[19] V. Jamali, D. S. Michalopoulos, M. Uysal, R. Schober, Link allocation for multiuser systems with hybrid RF/FSO backhaul: Delay-limited and delay-tolerant designs, IEEE Trans. Wireless Commun. 15 (5) (2016) 3281–3295.

[20] C. Abou-Rjeily, W. Fawaz, Buffer-aided relaying protocols for cooperative FSO communications, IEEE Trans. Wireless Commun. 16 (12) (2017) 8205–8219.

[21] C. Abou-Rjeily, W. Fawaz, Buffer-aided serial relaying for FSO communications: Asymptotic analysis and impact of relay placement, IEEE Trans. Wireless Commun. 17 (12) (2018) 8299–8313.

[22] M. Safari, M. Rad, M. Uysal, Multi-hop relaying over the atmospheric Poisson channel: Outage analysis and optimization, IEEE Trans. Commun. 60 (3) (2012) 817–829.

[23] S. Kazemlou, S. Hranilovic, S. Kumar, All-optical multihop free space optical communication systems, IEEE/OSA J. Lightwave Technol. 29 (18) (2011) 2663–2669.

[24] C. Abou-Rjeily, Power allocation for quantum-limited multihop free space optical communication systems, IEEE Commun. Lett. 16 (12) (2012) 2068–2071.

[25] S. M. Aghajanzadeh, M. Uysal, Multi-hop coherent free-space optical communications over atmospheric turbulence channels, IEEE Trans. Commun. 59 (6) (2011) 1657–1663.

[26] H. Sandalidis, T. Tsiftsis, G. Karagiannidis, Optical wireless communications with heterodyne detection over turbulence channels with pointing errors, IEEE/OSA J. Lightwave Technol. 27 (20) (2009) 4440–4445.

[27] A. Jurado-Navas, J. M. Garrido-Balsells, J. F. Paris, A. Puerta-Notario, J. Awrejcewicz, A unifying statistical model for atmospheric optical scintillation, Numerical Simulations of Physical and Engineering Processes (181) (2011).

[28] I. S. Ansari, F. Yilmaz, M. S. Alouini, Performance Analysis of Free-Space Optical Links Over Málaga ($\mathcal{M}$) Turbulence Channels With Pointing Errors, IEEE Trans. Wireless Commun., 15 (1) (2015) 91-102.